Cellular Signalling 127 (2025) 111616

Contents lists available at ScienceDirect

Cellular Signalling

journal homepage: www.elsevier.com/locate/cellsig

AP2A1 modulates cell states between senescence and rejuvenation

Pirawan Chantachotikul [a], Shiyou Liu [a], Kana Furukawa [a,b], Shinji Deguchi [a,b,c,*]

[a] Division of Bioengineering, Graduate School of Engineering Science, The University of Osaka, Japan
[b] R^3 Institute for Newly-Emerging Science Design, The University of Osaka, Japan
[c] Global Center for Medical Engineering and Informatics, The University of Osaka, Japan

ARTICLE INFO

Keywords:
Senescence
Rejuvenation
Cell size control
Stress ffbers
AP2A1
Focal adhesions

ABSTRACT

Aging proceeds with the accumulation of senescent cells in multiple organs. These cells exhibit increased size compared to young cells, which promotes further senescence and age-related diseases. Currently, the molecular mechanism behind the maintenance of such huge cell architecture undergoing senescence remains poorly understood. Here we focus on the reorganization of actin stress fibers induced upon replicative senescence in human fibroblasts, widely used as a senescent cell model. We identified, together with our previous proteomic study, that AP2A1 (alpha 1 adaptin subunit of the adaptor protein 2) is upregulated in senescent cells along the length of enlarged stress fibers. Knockdown of AP2A1 reversed senescence-associated phenotypes, exhibiting features of cellular rejuvenation, while its overexpression in young cells advanced senescence phenotypes. Similar functions of AP2A1 were identified in UV- or drug-induced senescence and were observed in epithelial cells as well. Furthermore, we found that AP2A1 is colocalized with integrin β1, and both proteins move linearly along stress fibers. With the observations that focal adhesions are enlarged in senescent cells and that this coincides with strengthened cell adhesion to the substrate, these results suggest that senescent cells maintain their large size by reinforcing their effective anchorage through integrin β1 translocation along stress fibers. This mechanism may work efficiently in senescent cells, compared with a case relying on random diffusion of integrin β1, given the enlarged cell size and resulting increase in travel time and distance for endocytosed vesicle transportation.

1. Introduction

Accumulation of senescent cells in multiple organs during aging contributes to age-associated diseases [1,2], which include neurodegenerative diseases [3,4], cardiovascular diseases [5,6], type 2 diabetes [7,8], and cancer [9,10]. Cultured human fibroblasts have been widely used in the study of cellular senescence as they exhibit a limited capacity for cell division before entering a stable proliferative growth arrest, a state known as "replicative senescence" [11]. The replicative senescence is caused by a telomere shortening upon each cell division, resulting in the accumulation of DNA damage [12]. Advanced senescence gradually leads to an increase in cell size [13], which in turn impairs cell function, proliferative ability, and protein synthesis [14]. Senescence is also accompanied by elevated activity of senescence-associated β-galactosidase (SA-β-gal) and expression of cell cycle inhibitors such as p53, p21, p16, and PAI-1 [15]. While cell morphological change is thus commonly recognized as a senescence indicator, the underlying mechanisms remain largely unknown. Replicative senescence also causes a decrease in cell migratory potential [16,17]. In this regard, the accumulation of senescent cells has been linked to impaired wound healing [18–20].

The regulation of cell morphology and migration is closely associated with the state of stress fibers [21,22]. Stress fibers are actomyosin-based bundles, which are composed mainly of actin filaments cross-linked by α-actinin and non-muscle myosin II [23–25]. In mesenchymal cell types, stress fibers localize between separate cell adhesion sites to generate contractile force on the underlying extracellular matrix [26,27]. Changes in stress fiber organization and contractile properties affect numerous cellular processes including adhesion [28,29], motility [30,31], and mechanosensing [23,32]. The organization of stress fibers, known to be altered in cells undergoing senescence [33,34], has also been reported to play a role in pathological processes including developmental morphogenesis and cancer metastasis [35,36].

While the proteome of stress fibers has only been partly investigated, our group recently revealed that those in human fibroblasts are comprised of at least 135 proteins, and 63 of them are upregulated with replicative senescence [37]. Approximately one-third of the upregulated

* Corresponding author at: 1-3 Machikane-yama, Toyonaka, Osaka 560-8531, Japan.
E-mail address: deguchi.shinji.es@osaka-u.ac.jp (S. Deguchi).

https://doi.org/10.1016/j.cellsig.2025.111616
Received 27 October 2023; Received in revised form 31 December 2024; Accepted 18 January 2025
Available online 21 January 2025

proteins belongs to the actin cytoskeletal component that includes caldesmon, tropomyosin, and filamin, which are all well characterized and are indeed likely to be enriched in the aged thick stress fibers; meanwhile, the function of the rest related to stress fibers remains unclear. Among them, here we focus on AP2A1 (alpha 1 adaptin subunit of the adaptor protein 2) because its molecular mechanisms behind the link to stress fiber regulation and cellular senescence have not been reported. AP2A1 is known to be a major protein involved in vesicle formation in clathrin-mediated endocytosis (CME) by recognizing and binding cargo proteins, clathrin, and accessory proteins [38–40]. AP2A1 has also been implicated in many diseases such as skin and neurodegenerative disorders [41], but their molecular details remain unclear.

Using human fibroblasts undergoing replicative senescence, we found that the expression level of AP2A1 modulates the extent of the senescence progression, specifically influencing the expression of senescence markers, morphological and migratory phenotypes, and thickness and turnover of individual stress fibers. Notably, knockdown of AP2A1 reversed senescence-associated phenotypes, exhibiting features of cellular rejuvenation. Similar functions of AP2A1 were identified not only in replicative senescence but also in UV- or drug-induced senescence and were found in epithelial cells as well as fibroblasts. We also showed that AP2A1 plays a role in integrin β1 translocation along the length of stress fibers, a process enhanced in aged fibroblasts to strengthen cell adhesions. Taken together, our study provided insights into the mechanisms behind the morphological alteration of stress fibers upon senescence and highlights AP2A1 as both a promising biomarker and a therapeutic target for promoting cellular rejuvenation.

2. Materials and methods

2.1. Cell culture

Primary human foreskin fibroblasts (HFF-1, ATCC) were cultured as a monolayer in high-glucose Dulbecco's Modified Eagle's Medium (DMEM, Wako) supplemented with 15 % fetal bovine serum (Sigma-Aldrich) and 1 % penicillin-streptomycin solution (Wako). Human mammary epithelial cells derived from normal breast tissue (MCF-10 A, ATCC) were cultured in DMEM/Ham's F12 medium (Wako) supplemented with 5 % horse serum (Gibco), 0.25 IU/ml of insulin (Wako), 0.5 mg/ml of hydrocortisone (Wako), 100 ng/ml of cholera toxin (Wako), 20 ng/ml of EGF (Wako), and 1 % of penicillin-streptomycin solution; cells were cultured starting from passage 2 and used for experiments at passage 4. Cells were kept at 37 °C in a humidified incubator with 5 % CO_2. The medium was changed once every 3 days, and cells were passaged at a split ratio of 1:3 for HFF-1 and 1:5 for MCF-10 A cells when 80 % confluence was reached.

2.2. SA-β-gal staining

Cell senescence was assessed by the senescence-associated β-galactosidase staining kit (Cell Signaling Technology) following the manufacturer's protocol. Briefly, cells at passage 10, 20, and 30 (hereafter described as P10, P20, and P30, respectively) were grown in 6-well plates until sub-confluence. Cells were fixed in 4 % paraformaldehyde in phosphate-buffered saline (PBS, Wako) at 37 °C after the media were removed and then were incubated with the β-galactosidase staining solution (pH 6.0) at 37 °C overnight in a dry incubator. Images were taken at 10 random fields using an inverted microscope (CKX 41, Olympus) to determine the percentage of SA-β-gal positive cells stained in blue.

2.3. Cell proliferation assay

Cell proliferation was assessed using the 5-Ethynyl-2-deoxyuridine (EdU) incorporation assay (Click-iT EdU Alexa Fluor 488 Imaging Kit or Click-iT EdU Alexa Fluor 647 Imaging Kit, Invitrogen) following the manufacturer's protocol. Briefly, cells were seeded on glass bottom dishes (Ø 27 mm, No. 1S, Iwaki) and treated with 20 μM EdU solutions diluted in culture media for 24 h at 37 °C. Cells were then fixed with 4 % paraformaldehyde, permeabilized with 0.5 % Triton X-100 in PBS for 20 min, and treated with Cu(I)-catalyzed click reaction cocktails for 30 min. Cells were also stained with Hoechst 33342 (5 μg/ml final concentration) in PBS. Stained cells were observed under a confocal laser scanning microscope (FV1000, Olympus) equipped with a UPlan Apo 10× objective lens. EdU-stained cells (proliferative cells) and Hoechst 33342-stained cells (total cells) were counted to evaluate the ratio of proliferative cells to the total cells.

2.4. Quantification of protein synthesis

To quantify protein synthesis, the Click-iT HPG Alexa Fluor 488 Protein Synthesis Assay Kit (Thermo Fisher Scientific) was used following the manufacturer's protocol, which evaluates the incorporation of L-homopropargylglycine (HPG) to newly synthetized proteins. Briefly, cells were incubated in methionine-free DMEM media for 1 h to deplete endogenous methionine and then in other methionine-free DMEM media containing 2 mM HPG for 30 min to allow incorporation of HPG to nascent proteins. Cells were then fixed and permeabilized for fluorescence imaging. The incorporation of HPG, quantified by the intensity of Alexa Fluor 488, was defined in each cell as the mean intensity of the pixels inside the cell boundaries after background subtraction.

2.5. Cellular ATP measurement

Intracellular ATP levels were measured using the ATP assay Kit-Luminescence (Dojindo Molecular Technologies) following the manufacturer's protocol. Briefly, 5000 cells in a well of 96-well plates were lysed with the lysis buffer of 50 μl and incubated at 25 °C for 10 min. Luminescence signals from the ATP standard solution and samples were detected on a microplate reader (SpectraMAX Gemini EM).

2.6. Immunostaining

Cells were seeded at a low density on coverslips, fixed with 4 % paraformaldehyde in PBS for 15 min, permeabilized with 0.5 % (*v/v*) Triton X-100 for 15 min, and blocked with 1 % (*w/v*) normal goat serum in PBS for 1 h at room temperature. Cells were then incubated overnight at 4 °C with primary antibodies, anti-AP2A1 (1:200, #MA1–064; Thermo Fisher Scientific), anti-vinculin (1:200, #ab11194; Abcam), anti-paxillin (1:200, #610569, BD Biosciences), anti-integrin β1 (1:200, #26918–1-AP; Proteintech Group), and anti-lysosomal-associated membrane protein-1 (LAMP-1, 1:200 #14–1079-80; Thermo Fisher Scientific), followed by incubation with secondary antibodies (anti-rabbit conjugated with Alexa Flour 488, anti-rabbit conjugated with Alexa Flour 546, anti-mouse conjugated with Alexa Flour 546; Invitrogen) for 2 h at 37 °C. To visualize stress fibers, cells were stained with phalloidin 488 (Funakoshi) or phalloidin 647 (Funakoshi) for 20 min at room temperature. Finally, cell nuclei were stained with Hoechst33342 (1 μg/ml final concentration), and samples were mounted with ProLong Gold Antifade Mountant (P36930, Thermo Fisher Scientific). Laser scanning confocal microscope (FV3000, Olympus) equipped with a UPlan Apo 60× oil objective lens (NA = 1.42) or 3D-structured illumination microscopy (SIM) (Zeiss Elyra S1; Center for Medical Innovation and Translational Research (COMIT) of Osaka University Medical School) equipped with an alpha Plan-Apochromat 100× oil objective lens (NA = 1.46) were used for imaging. For SIM, each image in the *z*-stack was captured with structured illumination at different focal depths, and the 3D image was reconstructed in super-resolution.

2.7. Quantification of cell area

The captured fluorescence images were imported to Fiji/ImageJ

software. After setting the scale, the cell contour was outlined by function "Polygon Selection", and then cell areas were measured by function Measure. Average values were obtained from measurements of n = 20–30 cells per experimental condition across N = 3 independent experiments.

2.8. Quantification of stress fiber thickness

Grey-scale images were used for fiber segmentation, which was performed in Fiji/ImageJ software by subtraction of non-uniform background within the cell boundaries. Line region of interest (ROI) was used to draw a ROI across the width of individual stress fibers. 2D graphs showing the intensities along the line selection were displayed to obtain the horizontal distance between the two edges of the stress fibers. The thickness of stress fibers was then determined as [(Peak intensity) – (Valley intensity)]/2. A total of more than 300 measurements were performed.

2.9. Fiber alignment analysis

Stress fibers and AP2A1 were imaged with confocal microscopy (FV3000) to evaluate their alignment using 2D-fast Fourier transform (FFT) in Fiji/ImageJ software. The FFT images provide a frequency map, in which the direction of the structure alignment is detected. Image components of high and low frequency, corresponding to short and long periodicity, are represented as peaks around the periphery and center in the Fourier spectrum, respectively. FFT-based directionality analysis (version 2.3.0) was used to assess the orientation and variability of stress fiber alignment. Results are presented as directionality histograms, with orientation angles on the *x*-axis and relative intensity on the *y*-axis. Alignment was quantified using the full width at half maximum (FWHM) of the histogram peak, which is determined automatically by fitting a Gaussian function, where smaller FWHM values indicate higher alignment.

2.10. Colocalization analysis

To analyze colocalization of endogenous proteins, including actin filaments, AP2A1, and transferrin, confocal microscopy images (resolution: 1024 × 1024 pixels, FV3000) were processed using the JACoP plugin in Fiji/ImageJ software. Cells were identified within manually selected ROI. The JACoP plugin quantifies the spatial and intensity relationships between two fluorescence signals in an image, using Pearson's correlation coefficient to assess the degree of colocalization.

2.11. Wound healing analysis

Cells were seeded in 12-well plates at a concentration of 1×10^5 cells/well and incubated until they reached 90 % confluence. A 200-μl sterile pipette tip was used to scratch the cells, and detached cells were removed with PBS. The plate was placed on a phase-contrast microscope (IX73, Olympus) to capture the resulting cell migration using a 4× objective every 30 min for 12 h. We determined the percentage of wound closure, namely the rate of cell migration, in Fiji/ImageJ software.

2.12. Single-cell tracking

Single-cell tracking was conducted using CellTracker Green CMFDA (Invitrogen)-labeled cells cultured on 35-mm glass-bottom dishes. Time-lapse imaging was performed with an IX-83 microscope (Olympus) equipped with a stage incubator (Tokai Hit) set at 37 °C and 5 % CO_2 in a humidified atmosphere. Images were captured at 10× magnification every 15 min over a 10-h period. Time-lapse fluorescence images were analyzed using the TrackMate plugin in Fiji/ImageJ to extract cell motion coordinates at each time point, yielding data on migration trajectories, velocity, and distance.

2.13. Transferrin uptake assay

Cells were grown on coverslips, pre-incubated with Opti-MEM (Gibco) for 2 h, incubated with Alexa-Fluor-488-conjugated transferrin of 25 μg/ml (Thermo Fisher Scientific) in Opti-MEM for 10 min on ice, shifted to 37 °C for 15 min to allow transferrin uptake, washed twice with PBS, and fixed with 4 % formaldehyde. The fluorescence images of cells were obtained using a confocal microscopy (FV3000) and analyzed with Fiji/ImageJ software to quantify transferrin uptake normalized to cell area. ROI representing specific cell areas were selected using the polygon tool.

2.14. Isolation of stress fibers

Stress fibers were isolated from cells as previous reported [37,42–44] Briefly, cells grown on 100-mm polystyrene cell culture dishes were washed twice with cold PBS, hypotonically shocked with a low-ionic-strength extraction solution (2.5 mM triethanolamine, 1 mM dithiothreitol, 1 μg/ml pepstatin, and 1 μg/ml leupeptin in ultra-pure water) for 5 min, incubated with 0.05 % Triton X-100 in the cytoskeleton stabilizing buffer (20 mM Imidazole, 2.2 mM $MgCl_2$, 2 mM EGTA, 13.3 mM KCl, 1 mM dithiothreitol, 1 μg/ml pepstatin, and 1 μg/ml leupeptin; pH 7.3) for 1 min, and rinsed with the same cytoskeleton stabilizing buffer without Triton X-100. The extracted stress fibers were scraped off from the dish, suspended in lysis buffer (50 mM Tris-HCl, 100 mM NaCl, 1 % NP-40, 1 % sodium deoxycholate, 1 mM Na_3VO_4, 1 mM NaF, 1 mM dithiothreitol, 1 mM phenylmethylsulfonyl fluoride, 1 μg/ml pepstatin, and 1 μg/ml leupeptin; pH 7.4). The stress fiber lysates were cleared by centrifugation (15,000 X*g*, 60 min) and were kept on ice for western blot analysis.

2.15. Western blotting

To prepare the whole cell extracts, cells were washed twice with cold PBS and scraped off using a plastic scraper from the culture dish containing lysis buffer. The lysates from the extracted stress fibers or whole cells were maintained on a shaker for 30 min at 4 °C and centrifuged at 15,000 X*g* for 20 min to collect the supernatant. The total protein concentration was determined by Pierce BCA Protein Assay Kit (Thermo Fischer Scientific). Proteins were fractionated by 10 % SDS-PAGE and transferred onto polyvinylidene fluoride membranes (0.45 μm, Wako). The membranes were blocked in 5 % (*w/v*) BSA for 1 h at room temperature, followed by incubation overnight at 4 °C with primary antibodies: anti-GAPDH (1:5000; #014–25,524; Wako), anti-p53 (1:1000; #10442–1-AP; Proteintech), anti-p21 (1:1000; #10355–1-AP; Proteintech), anti-myosin IIa (1:1000; #PRB-440P; Covance), anti-α-actinin (1:1000; #ab18061; Abcam), anti-β-actin (1:1000; #4970P; Cell Signaling Technology), and anti-AP2A1 (1:1000; #11401–1-AP; Proteintech). Excess antibodies were removed by washing with TBS-T three times. Membranes were then incubated with HRP-conjugated anti-rabbit/mouse for 1 h. After 3 washes with TBS-T, immunoreactive proteins were detected using Immobilon Western Kit (Millipore). Protein bands from each blot were observed by an imaging system (ChemiDoc XRS+) and analyzed by ImageLab software (Bio-rad). The GAPDH was used as an internal control.

2.16. Plasmids, transfection, and knockdown

An expression vector encoding mClover2-human AP2A1 was constructed from the pEX-A2-AP2A1 vector (Eurofins Genomics), which was digested with EcoRI and BamHI restriction enzymes and cloned into the EcoRI/BamHI-double-digested mClover2-C1 vector (Addgene plasmid#54577). Plasmid vectors for expressing human actin binding protein Lifeact (mRuby2-tagged Lifeact; [45]) and EGFP-tagged myosin

regulatory light chain (MLC; [32]), were generated as previously described. mVenus-Integrin-Beta1-N-18 plasmid (Addgene plasmid #56330) was obtained from Addgene (USA). Transfection was performed using Lipofectamine LTX and Plus reagent (Invitrogen) following the manufacturer's instructions with plasmids of 2.5 μg per well of 35-mm culture dishes where cells were grown to 50–70 % confluence in Opti-MEM medium. For co-transfection, the same amounts of two types of plasmids were applied to make 2.5 μg in total. Cell imaging was performed 24 h after transfection. The siRNAs targeting AP2A1 (s183 and s184, Thermo Fisher Scientific) and negative control siRNAs (Cell Signaling Technology) were transfected to cells to evaluate the effect of downregulating the expression of AP2A1. siRNA transfection was carried out at a concentration of 60 pmol in Opti-MEM medium using Lipofectamine RNAi-MAX (Invitrogen Life Technologies) following the manufacturer's instructions, and then cell imaging was performed 48 h after the transfection.

2.17. Fluorescence recovery after photobleaching (FRAP)

Fluorescence recovery after photobleaching (FRAP) was performed by using the laser scanning microscope (FV3000). Images were acquired using a 60× oil immersion objective lens (NA = 1.42) with line scanning. Two images were acquired to monitor the fluorescence signal before bleaching, and square areas of EGFP-MLC-labeled stress fibers were then photobleached using 405 and 488-nm wavelength lasers. The subsequent fluorescence recovery was recorded at a 20-s interval for 6 min.

2.18. Time-lapse imaging of protein transport

Cells at P10 and P30 were cotransfected with the two constructs: mClover2-AP2A1 (green) and mRuby2-tagged Lifeact (magenta) or mVenus-Integrin-Beta1 (green) and mRuby2-tagged Lifeact (magenta). Simultaneous time-lapse imaging of AP2A1 and integrin β1 along the length of stress fibers was recorded with confocal microscopy (FV3000) with a 30-s interval time for 10 min. To determine the speed of protein movement, we tracked AP2A1 and integrin β1 using TrackMate plugin in the Fiji/ImageJ software.

2.19. Induction of senescence by UV irradiation

Senescence was induced in young (P10) HFF-1 cells using a CSL-206G UVC lamp (Cosmo Bio). Cell culture dishes were positioned 14 cm from the light source and exposed to UVC irradiation for 10 min daily over a 3-day period. Under these conditions at room temperature, the UVC intensity at the cell surface was measured as 1400 μW/cm^2. Control cells were maintained under identical conditions except without UVC exposure. After the third day of treatment, cells were incubated for 24 h to recover from acute stress caused by UVC exposure before further experiments. For MCF-10 A cells, UVC treatment was performed under similar conditions with 10-min exposures daily for 2 days.

2.20. Induction of senescence by drug treatment

Cellular senescence was induced pharmacologically using two distinct drugs: Palbociclib (Sigma-Aldrich), i.e., a cyclin-dependent kinase 4/6 (CDK4/6) inhibitor, and Bleomycin (TCI), i.e., a DNA-damaging agent. Young (P10) HFF-1 cells were treated with 2 μM Palbociclib or 10 μg/ml Bleomycin, while MCF-10 A cells were exposed to 2 μM Palbociclib or 5 μg/ml Bleomycin. HFF-1 cells were cultured in drug-containing medium for 96 h, while MCF-10 A cells were treated for 72 h.

2.21. Statistical analysis

Each experiment was independently repeated at least three times, and results are expressed as means ± standard deviations. Statistical analyses were performed using GraphPad Prism (v.9.0.0) software. The statistical significance of differences among varying passage numbers, AP2A1 knockdown conditions (siControl, siAP2A1(1), siAP2A1(2)), and drug-induced senescence (control, Palbociclib treatment, Bleomycin treatment) was determined using a one-way analysis of variance (ANOVA), followed by Dennett's multiple comparison test. The significance between two experimental groups was analyzed using unpaired two-tailed Student's *t*-test. Statistical significance is described as follows: *, $p \leq 0.05$; **, $p \leq 0.01$; ***, $p \leq 0.001$; and, ****, $p \leq 0.0001$.

3. Results

3.1. Characterization of replicative senescent fibroblasts

Primary human foreskin fibroblast HFF-1 cells were expanded by serial passaging until passage 30 (P30) to induce replicative senescence. Cells at P10 were designated as young control, and those at P20 and P30 were categorized as the adult and aged cell groups, respectively. We found that cells at late passage exhibited an enlarged and flattened cell morphology (Fig. S1A). The area of aged cells (P30) increased by 6.6-fold compared to young control, whereas the nuclear size increased by 1.5-fold (Fig. S1A-B and Fig. S2A). With increasing the passage number, cells also underwent reduction in the aspect ratio from a spindle shape to an irregularly round one (Fig. S1C). We examined some senescence markers to determine how the large cell size is associated with senescence. As expected, enlarged cells at P30 exhibited senescence-specific characteristics, including a significant increase in SA-β-gal activity (Fig. S1D), delay in cell proliferation (Fig. S1E), upregulation of p53 and p21 (Fig. S1F), increase in cellular ATP levels (Fig. S2B), and down-regulation of protein synthesis (Fig. S2C) in accordance with previous studies on fibroblast replicative senescence [11,46,47].

3.2. Replicative senescence alters stress fiber organization

We next investigated how the above change in cell morphology is associated with stress fiber organization. Phalloidin staining revealed no significant difference in the number of individual stress fibers per 1000 μm^2 of cell area across passage numbers, while senescent cells exhibited increased stress fiber thickness compared to controls (Fig. S3A-C). To evaluate the alignment of stress fibers within cells, fluorescence images were analyzed using 2D-FFT (Fig. S4A). The directionality histogram of the FFT image of stress fibers in senescent cells shows a smaller FWHM around a specific angle, indicating a dominant orientation of stress fibers (Table S1). In contrast, the histogram of young cells is broad, reflecting a relatively random alignment. In addition, the expression level of typical stress fiber-associated proteins was determined by western blot analysis (Fig. S3D-E). We found that non-muscle myosin II (NMMIIa) and α-actinin are upregulated, while β-actin behaves as a house-keeping protein during the progression of senescence, thus consistent with our observations that the thickness of individual stress fibers is increased in senescent cells.

While stress fibers are highly dynamic and undergo continuous turnover, the thickening of individual stress fibers in senescent cells suggests increased structural stability with reduced turnover. To assess this, FRAP was performed on EGFP-MLC-transfected P10 and P30 cells (Fig. S3F). The fluorescence recovery curve after photobleaching reflects the extent of turnover (Fig. S3G). In senescent cells, recovery was markedly slower compared to young cells. At the endpoint ($t = 300$ s), the mobile fraction that represents the turnover proportion was significantly reduced in senescent cells (Fig. S3H), confirming that stress fibers in senescent cells are more stable with minimal turnover.

To investigate whether the progression of senescence affects cell migration, we analyzed both collective and single-cell migration. The wound healing assay revealed a significant reduction in the collective migration abiliity of senescent cells compared to young cells (Fig. S5A-C). Single-cell tracking showed that senescent cells exhibit decreased migration speed and total travel distance compared to young cells

(Fig. S6A-C and Movies 1-2). Together, these results indicate reduced motility in senescent cells, a hallmark of cellular senescence.

3.3. Upregulation of AP2A1 upon fibroblast replicative senescence

Previous proteomic data revealed that AP2A protein expression is upregulated in the stress fiber fraction in response to fibroblast replicative senescence [37]. To validate this finding with western blot, proteins from whole cell lysates and extracted stress fibers were analyzed at P10, P20, and P30. Consistent with the proteomic analysis, AP2A1 expression increased in both whole cell lysates and extracted stress fibers with the increase in passage number (Fig. 1A-D). Immunofluorescence staining was performed to investigate the localization of endogenous AP2A1 in cells (Fig. 1E). 2D-FFT analysis revealed a strong alignment of AP2A1 in senescent cells, contrasting with the more diffuse and random distributions observed in young cells (Fig. S4B). Notably, the alignment of AP2A1 closely matched that of stress fibers, with nearly identical angles (Tables S1 and S2). Quantitative colocalization analysis of AP2A1 and stress fibers in confocal images revealed a greater Pearson's correlation coefficient in senescent cells (Fig. 1F). 3D super-resolution SIM imaging provided more detailed observations, showing that the majority of AP2A1 protein localized just above or along individual stress fibers (Fig. 1G). These findings suggest that AP2A1 interacts along the surface of stress fibers.

As AP2A1 is known to be a major protein for vesicle formation in CME [39], we next investigated whether AP2A1 levels affect endocytosis using a transferrin endocytosis assay. The intarnalization of fluorescencently labeled transferrin was imaged, and quantitative analysis of fluorescence intensity and transferrin number per cell area revealed an increase in total cellular uptake with senescence (Fig. S7A-C). To establish the role of AP2A1 in endocytic trafficking, we analyzed its colocalization with transferrin. Quantification of fluorescence images showed that AP2A1 colocalizes with transferrin in both young and senescent cells, with a high value of Pearson's correlation coefficient (>0.7) and no significant difference between the two cell groups (Fig. S7D).

3.4. AP2A1 regulates cellular senescence

The concomitant upregulation of AP2A1 and senescence markers upon increased passage number led us to investigate the effects of knockdown and overexpression of AP2A1 on the phenotypes associated with cellular senescence. First, we used two different small interfering RNA (siRNA) sequences to deplete AP2A1 in senescent cells of P30. Upon silence of AP2A1, immunofluorescence showed that senescent cells exhibited a smaller cell area and thinner individual stress fibers compared to control (Fig. 2A-C). However, the number of individual stress fibers per 1000 μm^2 of cell area showed no significant difference between AP2A1 knockdown cells and control cells (Fig. 2D). Western blot showed that the expression of the major stress fiber-associated proteins, namely NMMIIa and α-actinin, was significantly reduced compared with control; meanwhile, β-actin remains unchanged (Fig. 2E-F). Interestingly, we found that the protein levels of p53 and p21 (Fig. 2G-H), as well as SA-β-gal activity (Fig. 2I-J), all of which are senescence markers, were downregulated by the knockdown of AP2A1 (Fig. 2A-B, G-H), while cell proliferation was enhanced (Fig. 2K-L). AP2A1 silencing was also found to significantly reduce transferrin receptor uptake (Fig. S8A-B).

In contrast, the overexpression of AP2A1 in young cells of P10 induced an increase in cell area (Fig. 3A-B) as well as the thickness of individual stress fibers (Fig. 3C) in a manner consistent with the upregulation of NMMIIa and α-actinin (Fig. 3D-E); meanwhile, β-actin expression was unaffected. However, the number of individual stress fibers per cell area remained unchanged (Fig. 3E). Furthermore, we observed that the protein levels of p53 and p21 (Fig. 3G-H) and SA-β-gal activity (Fig. 3I-J) were upregulated following AP2A1 overexpression, whereas cell proliferation was decreased (Fig. 3K-L). Given the opposite effects of AP2A1 knockdown and overexpression, which suppress and promote typical senescence phenotypes, respectively, these findings suggest that AP2A1 expression modulates cell states between senescence and rejuvenation.

3.5. Senescence promotes focal adhesions

Given that cells spread on the extracellular matrix (ECM) via integrin and form focal adhesions (FAs) to obtain a desirable state [48,49], it is hypothesized that increased cell area in senescence is accompanied by enhanced structural maturity of FAs. To examine this relationship, we examined by immunostaining the expression of FA-associated proteins, vinculin and paxillin, in both young and senescent cell groups. Cells in each group were divided into two regions: edge and non-edge. The edge was defined as the intracellular region within 10 % of the distance from the cell outline to the center, while the remaining intracellular regions were defined as non-edge. The number and size of individual FAs were quantified for each cell group, showing that in young cells both vinculin and paxillin are preferentially distributed around the cell edge, whereas in senescent cells those proteins were rather located at the cell center (Fig. 4A-B, Table S3). Stress fibers in young and senescent cells likewise tend to be located around the periphery and central regions of the cells, respectively (Fig. S9). The size of individual FAs was significantly larger in senescent cells compared to young cells (Fig. 4C-D), suggesting that cellular senescence exhibiting increased cell area is accompanied by the maturity of FAs.

We further investigated how the cell adhesions to the ECM is strengthened during senescence by using trypsin-based cell detachment assay. Here, the resistance to trypsin reflects how firmly cells attached to the substrate as the ECM associated with cell adhesions is known to be developed together with the SF-driven maturation of FAs [50–52] The time required for de-adhesion with trypsinization was significantly delayed in senescent cells compared to young cells (Fig. S10). Thus, FAs in senescent cells are not only augmented in size and molecular expression but also strengthened in terms of anchorage to the ECM.

3.6. AP2A1 is required for integrin β1 translocation

Endocytosis of vesicles carrying integrin β1 via CME has been proposed to be a mechanism to supply integrin for newly forming FAs [53-55]. Based on the above results that FAs are strengthened upon senescence, we hypothesized that AP2A1 is involved in translation of integrin β1 along the length of stress fibers. To test this, we first performed double immunofluorescence staining of AP2A1 and integrin β1. The 3D-SIM images demonstrate partial colocalization of integrin β1 and AP2A1, with a high Pearson's correlation coefficient of over 0.5, while there is no significant difference in the extent between young and senescent cell groups (Fig. 4E-F). Integrin β1 may be recycled back to the plasma membrane via endosomes or targeted for degradation at lysosomes, namely autophagy [56]. In this regard, we analyzed the colocalization of integrin β1 with the lysosome marker, LAMP1. We observed a decrease in the integrin β1 overlap with LAMP1 upon senescence (Fig. S11A-B). These results inspired us to consider that senescent cells tend to promote the recycle of internalized integrin β1 back to the plasma membrane as a potential new resource to maintain FAs, while young cells rather allow internalized integrin β1 to be transported to degradative lysosomes. Moreover, the accumulation of integrin β1 was quantified by taking the ratio of integrin β1 intensity at P30 to that at P10, showing that it significantly increases more than twice at P30 compared to P10 (Fig. 4G).

To analyze the involvement of AP2A1 in integrin β1 transportation, living cells transfected with EGFP-AP2A1 and mRuby-Lifeact were imaged by time-lapse confocal microscopy at an interval of 30 s for 10 min. The fluorescence of individual AP2A1 aggregations was tracked to demonstrate that AP2A1 moves along the length of stress fibers (Movies

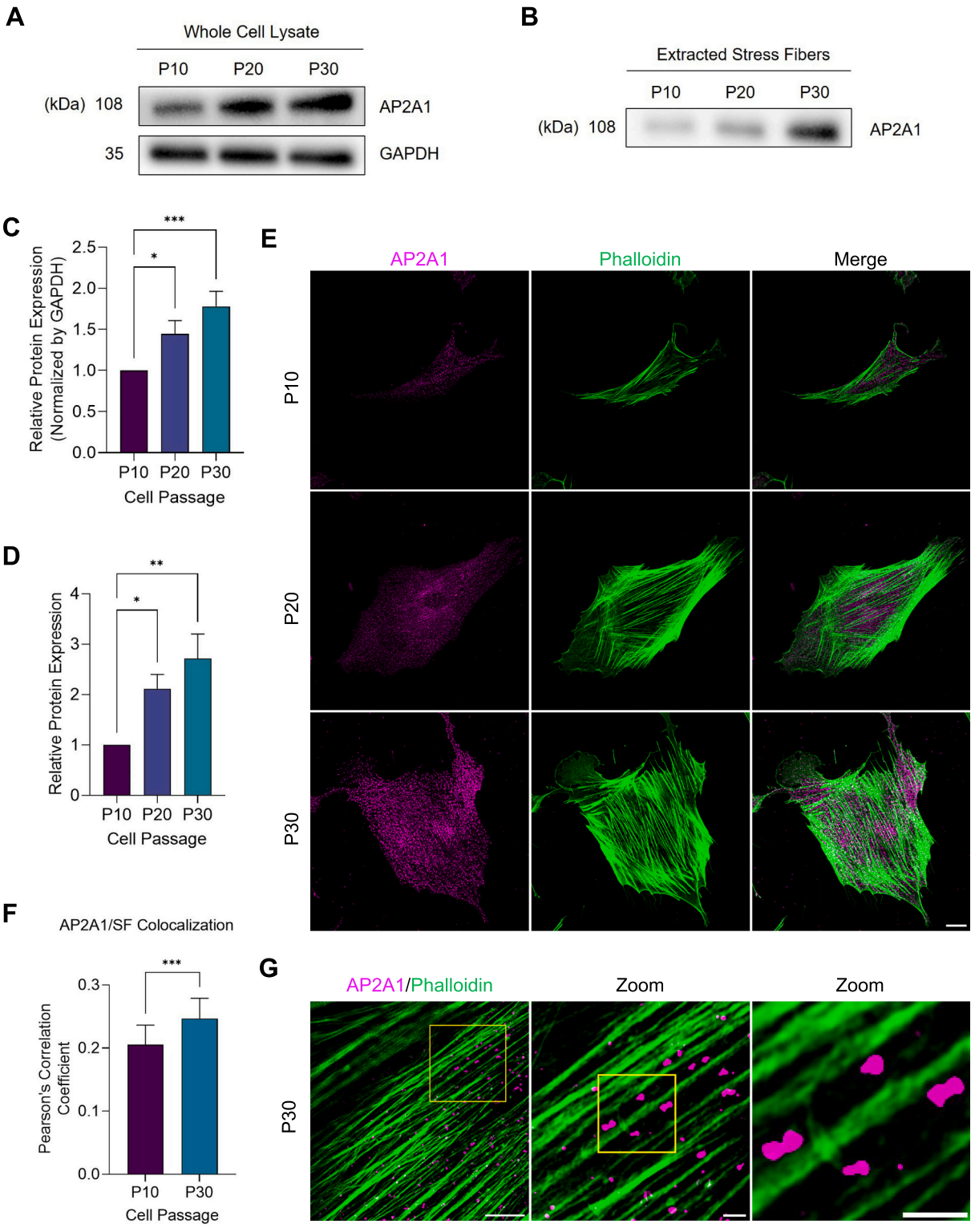

Fig. 1. Increased AP2A1 protein expression in senescent cells. (A, B) Western blot of AP2A1 in the whole cell lysate (A; $N = 3$ independent experiments) and in extracted stress fibers (B; $N = 3$ independent experiments). (C, D) Quantification of the expression of AP2A1 in the whole cell lysates (C) and extracted stress fibers (D). (E) Immunostaining of endogenous AP2A1 (magenta) and actin filaments in stress fibers (phalloidin, green). (F) Pearson's correlation coefficient to evaluate colocalization of AP2A1 and actin filaments ($n = 20$ cells). (G) 3D-reconstructed SIM image of AP2A1 and actin filaments in stress fibers (phalloidin) in P30 cell. The rectangles in yellow are magnified to show the detail. Scale, 5 μm; 1 μm for the magnified images. (For interpretation of the references to colour in this figure legend, the reader is referred to the web version of this article.)

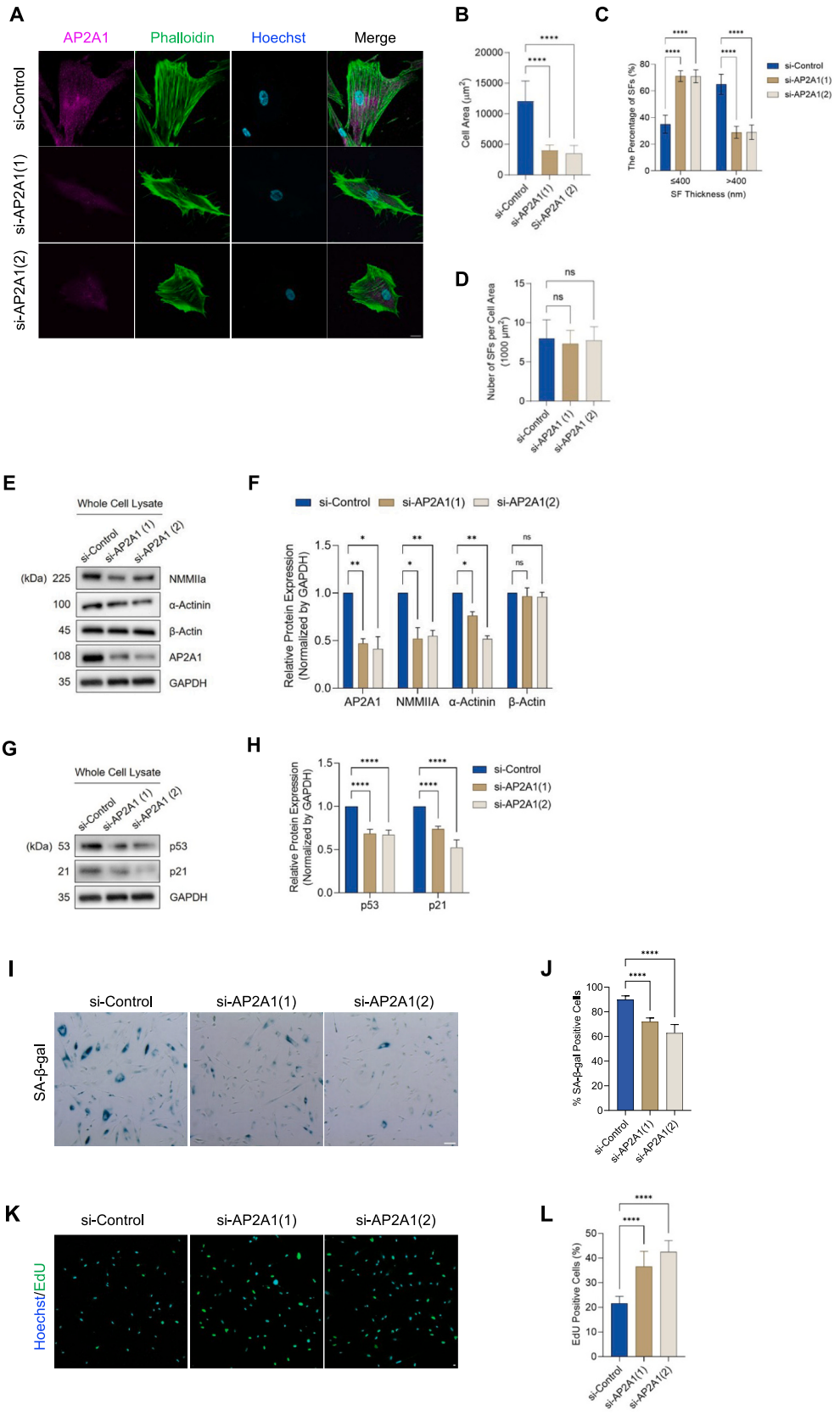

(caption on next page)

Fig. 2. AP2A1 knockdown promotes features of cellular rejuvenation. (A) Immunostaining of AP2A1 (magenta), actin filaments in stress fibers (phalloidin, green), and nuclei (Hoechst33342, blue) in senescent P30 cells with si-control or si-AP2A1 transfection. Scale, 20 μm. (B) Quantification of cell area ($n = 30$ cells, $N = 3$ independent experiments). (C, D) Quantification shows the thickness (C) and the number of individual stress fibers (SFs) per cell area (D) under the knockdown ($n =$ 20 cells for each group from 3 independent experiments). (E, F) Western blot shows that AP2A1 knockdown in P30 cells led to a reduced expression of NMMIIa and α-actinin. (G, H) Western blot shows that the expression of p53 and p21 was both reduced by AP2A1 knockdown. The blots are representative of $N = 3$ independent experiments. (I, J) Representative images of P30 cells with SA-β-gal staining (I) and its quantification (J). Scale, 100 μm. ($n = 10$ random fields for each group, $N = 3$ independent experiments). (*K*,*L*) Comparison of cell proliferation ability between senescent cells expressing siRNA for control and for AP2A1 by EdU proliferation assay (K) and its quantification (L). Scale, 20 μm. ($n = 10$ random fields for each group, $N = 3$ independent experiments). (For interpretation of the references to colour in this figure legend, the reader is referred to the web version of this article.)

3–4). The speed of AP2A1 movement was significantly faster in young cells compared to senescent cells (Fig. 5A-B). Using the same approach, we also observed integrin β1 translocation along stress fibers in cells transfected with mVenus-integrin β1 and mRuby-Lifeact (Movies 5–6). The integrin β1 movement was substantially faster in young cells, consistent with the observation of the AP2A1 dynamics (Fig. 5C-D). These data support our hypothesis that integrin β1 contained in a vesicle with AP2A1 is translocated by CME along stress fibers to FAs where integrin β1 is clustered (Fig. 5E), and the turnover rate of integrin β1 is slowed in senescent cells as the associated stress fibers are stabilized (Fig. S3F-H).

3.7. Upregulation of AP2A1 in alternative fibroblast senescence models

To further validate the upregulation of AP2A1 in senescent fibroblasts, young cells at P10 were treated with UVC irradiation or specific drugs. UVC exposure induced senescence, as evidenced by enlarged and flattened cell morphology (Fig. S12A–B) and increased SA-β-gal activity (Fig. S12C-D). Immunofluorescence analysis revealed increased AP2A1 expression (Fig. S12E–F) and stress fiber thickness in UV-treated HFF-1 cells compared to controls, while the number of individual stress fibers per cell area remained unchanged (Fig. S13G–H).

Fibroblast senescence was also induced by treating young HFF-1 cells with Palbociclib (CDK4/6 inhibitor) or Bleomycin (DNA-cleaving agent). These drug treatments resulted in increased cell area and SA-β-gal staining (Fig. S13A–D). Drug-treated fibroblasts exhibited significant upregulation of AP2A1 expression (Fig. S13E–F) and increased stress fiber thickness, while no significant change was observed in the number of individual stress fibers per cell area (Fig. S13G–H). Collectively, AP2A1 serves as a marker for fibroblast senescence not only in replicative models but also in UV- and drug-induced senescence models.

3.8. Upregulation of AP2A1 in epithelial cell senescence

We next investigated whether AP2A1 could serve as a senescence marker in other cell types. MCF-10 A cells were exposed to UVC irradiation, Palbociclib, or Bleomycin and assessed for senescence. UV treatment induced senescence in MCF-10 A cells, as evidenced by increased cell spreading with an elongated shape (Fig. S14A–B) and elevated SA-β-gal activity (Fig. S14C–D). Compared to controls, AP2A1 expression was significantly upregulated in UV-treated cells (Fig. S14E–F). Quantitative analysis revealed increases in both the number and thickness of individual stress fibers, along with a loss of cell–cell contacts (Fig. S14G-H).

Similarly, Palbociclib and Bleomycin treatment induced senescence in MCF-10 A cells. Drug-treated cells exhibited cell enlargement (Fig. S15A–B) and increased SA-β-gal activity (Fig. S15C–D). A significant upregulation of AP2A1 expression was observed compared to controls (Fig. S15E-F). Quantitative analysis confirmed increases in both the number and thickness of individual stress fibers following drug treatment (Fig. S15G-H). Collectively, AP2A1 is upregulated in senescent MCF-10 A cells, supporting its role as a senescence marker across different cell types.

4. Discussion

The function of organisms progressively declines during the lifespan due to overaccumulation of senescent cells in multiple tissues, leading to age-related diseases [57,58]. Many researches have attempted to develop therapeutic drugs targeting senescent cells, and cultured human fibroblasts are often used in those studies as an in vitro model to induce cellular senescence [11,59,60]. In the present study, we established a replicative senescence model of HFF-1 cells by serial passage. Cells at P30 exhibited typical senescence characteristics, e.g., an enlarged and flattened cell shape, increased SA-β-galactosidase activity, and upregulated p53 and p21 (Fig. S1), thus consistent with previous studies [61–63]. Many studies on senescence have also reported that cell size increases gradually during replicative senescence [64,65], and alteration in cell size contributes to decline in cell function, proliferation, and protein synthesis [14,66]. However, there is little understanding of the mechanism behind the significant changes in stress fibers as well as FAs that are known to be elicited upon replicative senescence.

We found that major senescence phenotypes are indeed induced to the human fibroblasts with repeated passage, in which stress fibers were thickened (Fig. S1-S3). In the aged stress fibers, higher expression levels of actin-binding proteins, specifically, NMMIIa and α-actinin, are associated compared to control young stress fibers. The FRAP analysis showed reduced stress fiber turnover in senescent cells, indicating their stabilization during senescence. Given the association of stress fibers with cell migration [67], we investigated the effect of expressing the stabilized stress fiber organization on cell migration and found that it slows cell migration (Fig. S5-S6).

Toward better understanding of senescence-related change in stress fiber organization, our group previously conducted proteomic analysis on HFF-1 cells with or without replicative senescence, identifying that 63 different proteins are upregulated along stress fibers in response to induced senescence [37]. Approximately two-thirds of them are not known for the function related to stress fibers as well as how it plays a role in senescence, and therefore among them here we focused on AP2A1. We confirmed the upregulation of endogenous AP2A1 along stress fibers in the same human fibroblasts HFF-1 cells upon senescence progression by western blot and immunostaining (Fig. 1). AP2A1 has been implicated as a potential biomarker among patients with ovarian cancer [68], pediatric medulloblastoma [69], and Alzheimer's disease [70,71]. Although AP2A1 was thus suggested to be a pathological marker for aging-associated diseases, the underlying mechanisms were yet to be identified [39]. In this regard, we demonstrated that AP2A1 plays a role in cellular senescence by modulating the size of individual stress fibers and FAs. The aberrant expression of AP2A1 in senescent cells may result from an increased total cellular uptake surface area [72] and prolonged travel time [73] and distance for endocytosed vesicle transport, as discussed further below.

We demonstrated that AP2A1 knockdown in senescent cells reduces major senescence markers and phenotypes (Fig. 2), while its overexpression in young cells promotes them (Fig. 3). The term "rejuvenation" is often used to describe consistent reductions in aging markers and evidence of functional recovery, such as enhanced migration or cell cycle reentry demonstrated by EdU incorporation [74,75]. In this context, our findings suggest that AP2A1 not only influences morphological alterations and stress fiber reorganization in senescent cells but

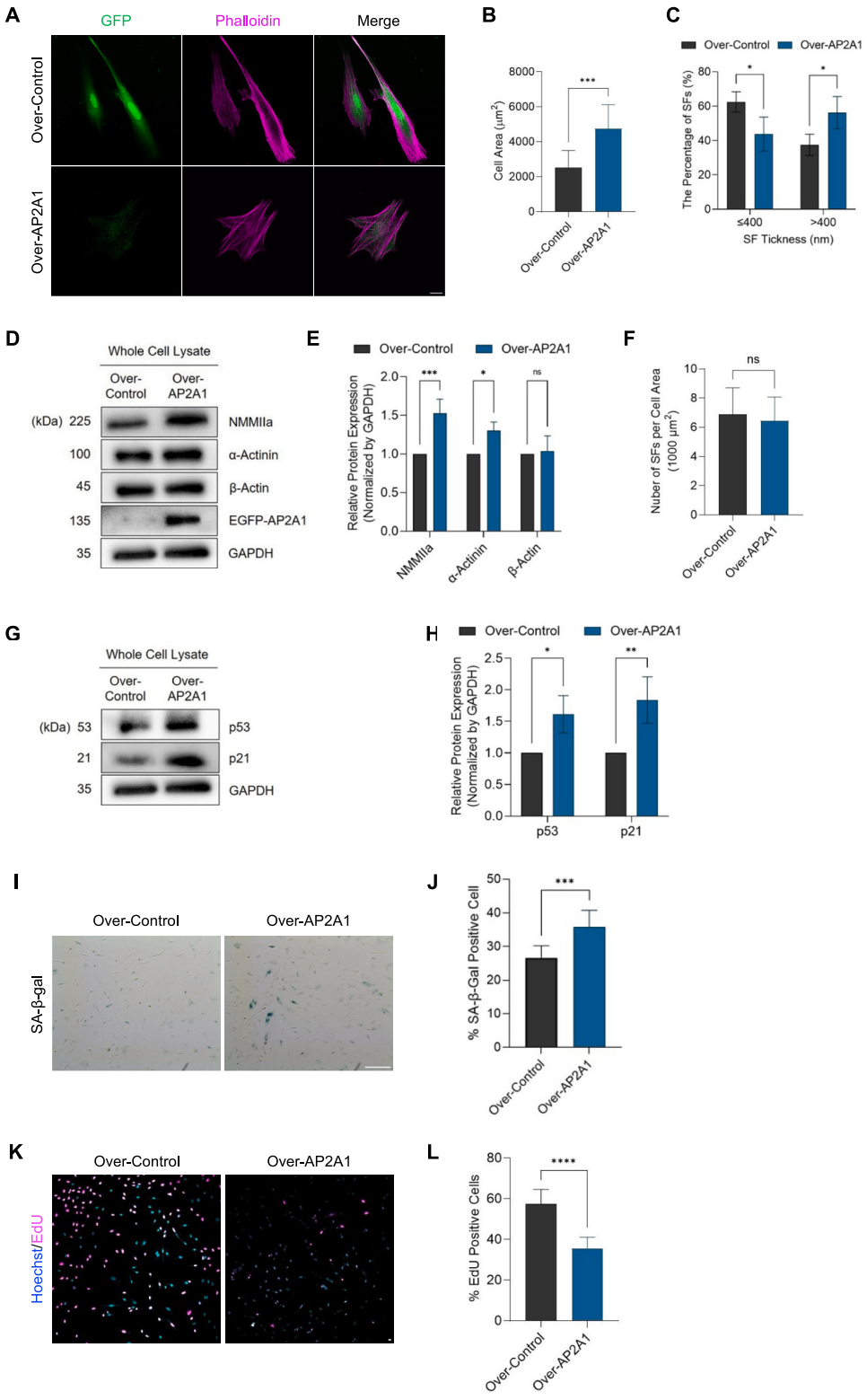

Fig. 3. AP2A1 overexpression in young cells promotes senescence. (A) Fluorescence images of EGFP (AP2A1, green) and phalloidin (actin filaments, magenta) for cells with EGFP-AP2A1 overexpression. Scale, 20 μm. (B) Quantification of cell area ($n = 30$ cells, $N = 3$ independent experiments) (C) Quantification shows the thickness of individual stress fibers under the overexpression ($n = 30$ cells for each group). (D, E) Western blot of major stress fiber-associated proteins and AP2A1 (D) and its quantification (E). (F) Quantification shows the thickness of individual stress fibers under the overexpression ($n = 30$ cells for each group). (G, H) Western blot of senescence markers (G) and its quantification (H). The blots are representative of $N = 3$ independent experiments. (I, J) Representative images of P10 cells with SA-β-gal staining (I) and its quantification (J). Scale, 100 μm. ($n = 10$ random fields for each group, $N = 3$ independent experiments). (K, L) Comparison of cell proliferation ability between young cells overexpressing AP2A1 and control by EdU proliferation assay (K) and its quantification (L). Scale, 20 μm. ($n = 10$ random fields for each group, $N = 3$ independent experiments). (For interpretation of the references to colour in this figure legend, the reader is referred to the web version of this article.)

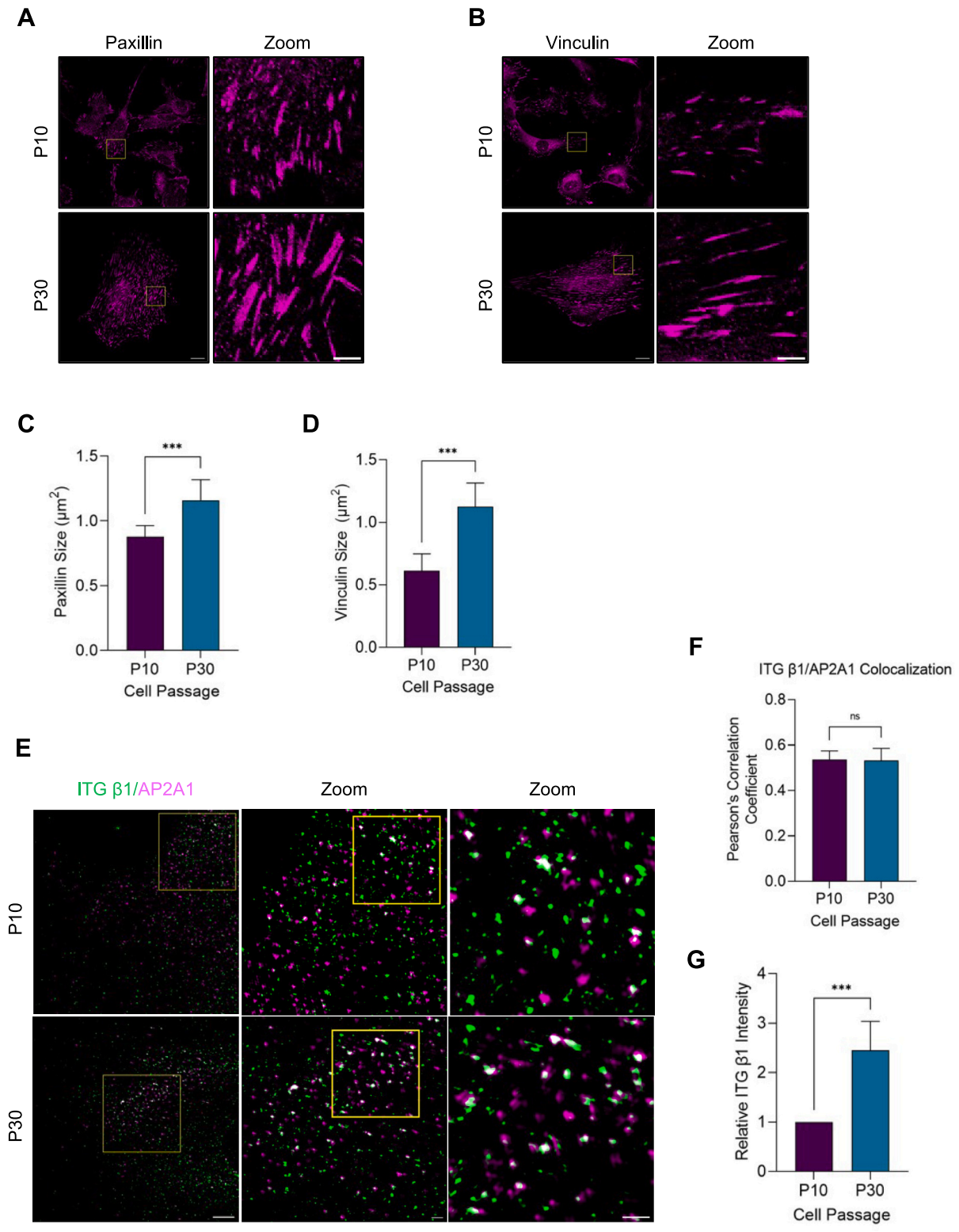

Fig. 4. Focal adhesion maturation in response to senescence. (A, B) Immunostaining of paxillin (A) and vinculin (B) in P10 and P30 cells. Scale, 20 μm; 5 μm for the magnified images. (C, D) Quantification of the area of individual FAs determined by the paxillin (C) and vinculin (D) images ($n = 30$ cells for each group from $N = 3$ independent experiments). (E) Representative 3D-reconstructed SIM image of integrin β1 and AP2A1 in P10 and P30 cells. The rectangles in yellow are magnified to show the detail. Scale, 5 μm; 1 μm for the magnified images. (F) Quantification of the colocalization of integrin β1 and AP2A1 ($n = 20$ cells for each group $N = 3$ independent experiments). (G) Quantification of the ratio of integrin β1 fluorescence intensity at P30 ($n = 20$ cells) to that at P10 ($n = 20$ cells). (For interpretation of the references to colour in this figure legend, the reader is referred to the web version of this article.)

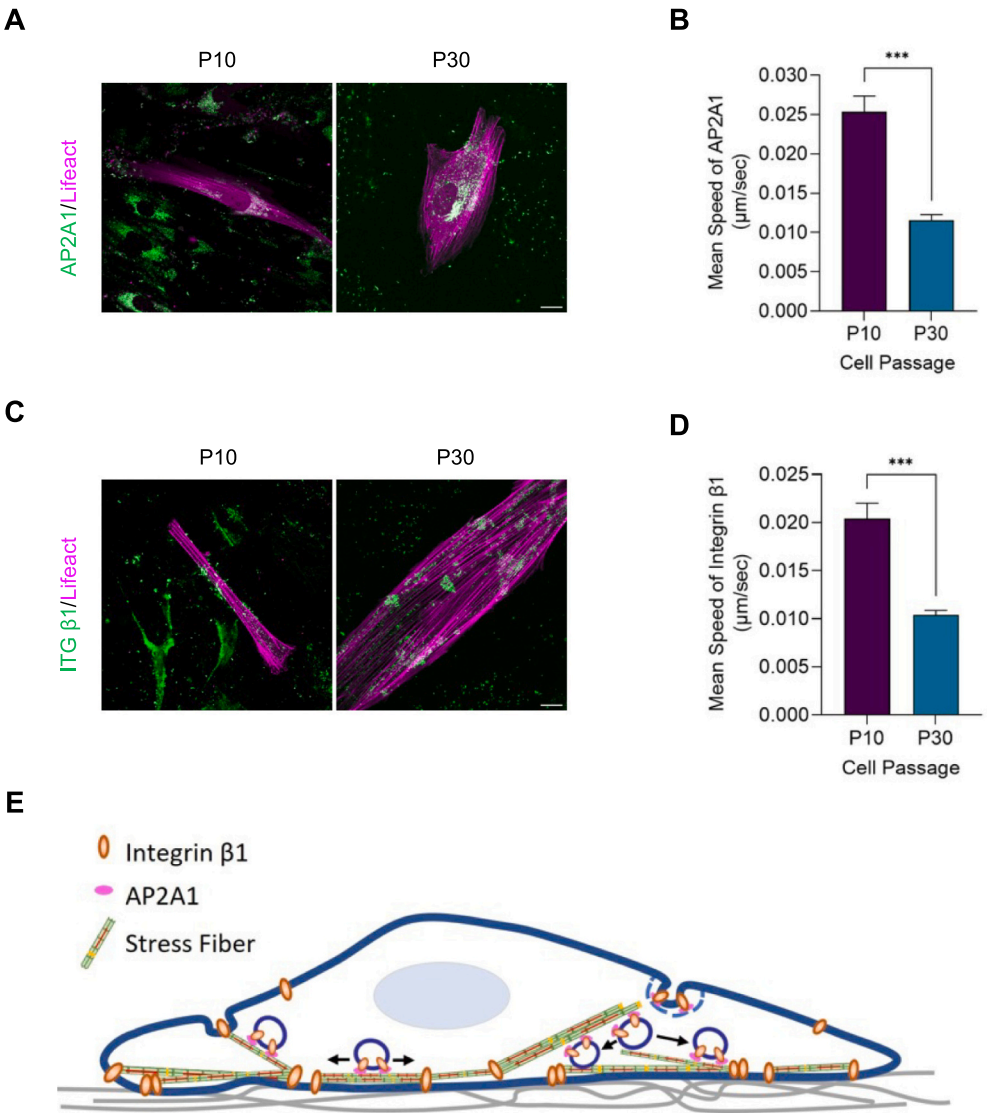

Fig. 5. Analysis of protein movement along stress fibers. (A) Snapshot of Movies 3–4, in which EGFP-AP2A1 (green) and mRuby2-Lifeact (magenta) were expressed in P10 and P30 cells to observe the movement. (B) Quantification of the speed of AP2A1 movement ($n = 30$) (C) Snapshot of Movies 5–6, in which mVenus-integrin β1 (green) and mRuby2-Lifeact (magenta) were expressed in P10 and P30 cells to observe the movement. (D) Quantification of the speed of integrin β1 movement ($n = 30$). (E) Schematic of integrin β1 translocation along stress fibers via CME. (For interpretation of the references to colour in this figure legend, the reader is referred to the web version of this article.)

also modulates senescence progression, with knockdown promoting features of cellular rejuvenation and overexpression driving senescence. It is therefore of interest to identify the molecule transported by AP2A1 that controls the senescence phenotype.

Cell adhesion, spreading, and migration on the substrate are modulated by the integrin-mediated formation of FA complexes [76–78]. Our observation that extensively spread senescent cells express highly mature FAs with a large size (Fig. 4A-D) led us to focus on integrin endocytic trafficking. The integrin αβ heterodimers play a crucial role in cell-matrix attachment, and the majority of integrin receptors associated with stress fibers contain the β1 subunit [79]. Under certain conditions, integrin adhesions are highly dynamic, undergoing continuous cycles of assembly and disassembly to facilitate the regulation of cell adhesion. The main integrin internalization route is via CME [80,81]. Given these reports, our observations on the colocalization of integrin β1 and AP2A1 required for the CME suggest that AP2A1, becoming associated with stress fibers in senescent cells, is involved in vesicle-bound integrin β1 transportation in the senescent state. In fact, it has been reported that in fibroblasts fibronectin-bound integrin α5β1 translocates along stress fibers [82]. The movement of vesicles over a long range along stress fibers is mediated by myosin 5b [83]. Other studies demonstrated translocation of vesicles containing integrin from the intracellular space to the extending tip of cell adhesions by stress fiber-dependent translocation [84,85]. All heterodimers containing integrin β1 have thus been shown to be potentially endocytosed via the same mechanism [86,87]. In addition, autophagy, namely a lysosome-dependent cellular degradation process, works as another regulator of integrin-mediated cell adhesion [88]. Particularly, suppression of autophagy has been implicated in cellular senescence [65]. Thus, integrin can be recycled back to the plasma membrane after internalization or degraded in lysosomes via autophagy [56]. We observed downregulation of integrin β1 degradation and stabilized translocation of integrin along stress fibers in senescent cells (Figs. 4 and S11), supporting enhanced integrin recycling rather than degradation. The integrin translocation along stress fibers may be efficient to maintain FAs in senescent cells, instead of transporting the molecules in a random diffusion-limited manner, given the greatly enlarged cell volume and resulting increase in travel time and distance for endocytosed vesicle transportation (Fig. 5E).

Taken together, we elucidated key molecular mechanisms behind cell enlargement in replicative senescence; specifically, aged fibroblasts exhibit enhanced integrin β1 translocation along stress fibers toward FAs, which requires AP2A1 to form the necessary vesicles. We propose a mechanistic explanation that individual FAs are significantly enlarged in senescent cells to ensure firm anchorage to the substrate enough to sustain the large cell architecture. We also demonstrated that AP2A1 expression is upregulated in both UV- and drug-induced senescent fibroblasts and epithelial cells. This upregulation is accompanied by senescence-associated morphological changes, increased SA-β-gal activity, and enhanced stress fiber formation. Given its significant role in modulating senescence progression and rejuvenation, our findings suggest that AP2A1 may serve as a novel senescence marker and a potential therapeutic target for age-related diseases.

Supplementary data to this article can be found online at https://doi.org/10.1016/j.cellsig.2025.111616.

Funding

This study was partly supported by JSPS KAKENHI grant (21H03796 and 23H04929) and JICA (Japan International Cooperation Agency).

CRediT authorship contribution statement

Pirawan Chantachotikul: Conceptualization, Data curation, Formal analysis, Investigation, Methodology, Validation, Visualization, Writing – original draft, Writing – review & editing. **Shiyou Liu:** Data curation, Resources. **Kana Furukawa:** Resources. **Shinji Deguchi:** Conceptualization, Data curation, Methodology, Project administration, Resources, Supervision, Validation, Visualization, Writing – review & editing.

Declaration of competing interest

The authors declare no competing or financial interests.

Acknowledgments

The authors thank Natsuki Saito and Shinji Sakai (The University of Osaka) for their assistance in cellular ATP measurement.

Data availability

All relevant data can be found within the article and its supplementary information.

References

[1] J.M. Phillip, I. Aifuwa, J. Walston, D. Wirtz, The Mechanobiology of aging, Annu. Rev. Biomed. Eng. 17 (2015) 113–141.
[2] F.A. Valentijn, L.L. Falke, T.Q. Nguyen, R. Goldschmeding, Cellular senescence in the aging and diseased kidney, J. Cell. Commun. Signal. 12 (1) (2018) 69–82.
[3] M. Kritsilis, S.V. Rizou, P.N. Koutsoudaki, K. Evangelou, V.G. Gorgoulis, D. Papadopoulos, Ageing, cellular senescence and neurodegenerative disease, Int. J. Mol. Sci. 19 (10) (2018) 2937, https://doi.org/10.3390/ijms19102937.
[4] C. Martínez-Cué, N. Rueda, Cellular senescence in neurodegenerative diseases, Front. Cell. Neurosci. 14 (2020) 16.
[5] F. Olivieri, R. Recchioni, F. Marcheselli, A.M. Abbatecola, G. Santini, G. Borghetti, R. Antonicelli, A.D. Procopio, Cellular senescence in cardiovascular diseases: potential age-related mechanisms and implications for treatment, Curr. Pharm. Des. 19 (9) (2013) 1710–1719.
[6] B.G. Childs, H. Li, J.M. van Deursen, Senescent cells: a therapeutic target for cardiovascular disease, J. Clin. Invest. 128 (4) (2018) 1217–1228.
[7] A.K. Palmer, B. Gustafson, J.L. Kirkland, U. Smith, Cellular senescence: at the nexus between ageing and diabetes, Diabetologia 62 (10) (2019) 1835–1841.
[8] H. Shakeri, K. Lemmens, A.B. Gevaert, G.R.Y. De Meyer, V.F.M. Segers, Cellular senescence links aging and diabetes in cardiovascular disease, Am. J. Phys. Heart Circ. Phys. 315 (3) (2018) H448–H462.
[9] J. Campisi, Aging, cellular senescence, and Cancer, Annu. Rev. Physiol. 75 (1) (2013) 685–705.
[10] A. Krtolica, S. Parrinello, S. Lockett, P.-Y. Desprez, J. Campisi, Senescent fibroblasts promote epithelial cell growth and tumorigenesis: a link between cancer and aging, Proc. Natl. Acad. Sci. 98 (21) (2001) 12072–12077.
[11] L. Hayflick, P.S. Moorhead, The serial cultivation of human diploid cell strains, Exp. Cell Res. 25 (1961) 585–621.
[12] S. Courtois-Cox, S.L. Jones, K. Cichowski, Many roads lead to oncogene-induced senescence, Oncogene 27 (20) (2008) 2801–2809.
[13] M. Narita, S. Nünez, E. Heard, M. Narita, A.W. Lin, S.A. Hearn, D.L. Spector, G. J. Hannon, S.W. Lowe, Rb-mediated heterochromatin formation and silencing of E2F target genes during cellular senescence, Cell 113 (6) (2003) 703–716.
[14] G.E. Neurohr, R.L. Terry, J. Lengefeld, M. Bonney, G.P. Brittingham, F. Moretto, T. P. Miettinen, L.P. Vaites, L.M. Soares, J.A. Paulo, J.W. Harper, S. Buratowski, S. Manalis, F.J. van Werven, L.J. Holt, A. Amon, Excessive cell growth causes cytoplasm dilution and contributes to senescence, Cell 176 (5) (2019) 1083–1097, e18.
[15] A. Calcinotto, A. Alimonti, Aging tumour cells to cure cancer: "pro-senescence" therapy for cancer, Swiss Med. Wkly. 147 (2017) w14367.
[16] S. Geissler, M. Textor, J. Kühnisch, D. Könnig, O. Klein, A. Ode, T. Pfitzner, J. Adjaye, G. Kasper, G.N. Duda, Functional comparison of chronological and in vitro aging: differential role of the cytoskeleton and mitochondria in mesenchymal stromal cells, PLoS One 7 (12) (2012) e52700.
[17] L.T. Younis, M.I. Abu Hassan, T.B. Taiyeb Ali, T.J. Bustami, 3D TECA hydrogel reduces cellular senescence and enhances fibroblasts migration in wound healing, Asian, J. Pharm. Sci. 13 (4) (2018) 317–325.
[18] G.D. Mulder, J.S. Vande Berg, Cellular senescence and matrix metalloproteinase activity in chronic wounds. Relevance to debridement and new technologies, J. Am. Podiatr. Med. Assoc. 92 (1) (2002) 34–37.
[19] D. Telgenhoff, B. Shroot, Cellular senescence mechanisms in chronic wound healing, Cell Death Differ. 12 (7) (2005) 695–698.
[20] A. Stanley, T. Osler, Senescence and the healing rates of venous ulcers, J. Vasc. Surg. 33 (6) (2001) 1206–1211.
[21] E. Kassianidou, S. Kumar, A biomechanical perspective on stress fiber structure and function, Biochimica et Biophysica Acta (BBA), Mol. Cell Res. 1853 (11, Part B) (2015) 3065–3074.
[22] M. Vicente-Manzanares, M.A. Koach, L. Whitmore, M.L. Lamers, A.F. Horwitz, Segregation and activation of myosin IIB creates a rear in migrating cells, J. Cell Biol. 183 (3) (2008) 543–554.
[23] K. Burridge, E.S. Wittchen, The tension mounts: stress fibers as force-generating mechanotransducers, J. Cell Biol. 200 (1) (2013) 9–19.
[24] L.P. Cramer, M. Siebert, T.J. Mitchison, Identification of novel graded polarity actin filament bundles in locomoting heart fibroblasts: implications for the generation of motile force, J. Cell Biol. 136 (6) (1997) 1287–1305.
[25] E. Lazarides, K. Burridge, Alpha-actinin: immunofluorescent localization of a muscle structural protein in nonmuscle cells, Cell 6 (3) (1975) 289–298.
[26] K. Burridge, C. Guilluy, Focal adhesions, stress fibers and mechanical tension, Exp. Cell Res. 343 (1) (2016) 14–20.
[27] H. Li, D. Matsunaga, T.S. Matsui, H. Aosaki, G. Kinoshita, K. Inoue, A. Doostmohammadi, S. Deguchi, Wrinkle force microscopy: a machine learning based approach to predict cell mechanics from images, Commun. Biol. 5 (1) (2022) 361.
[28] B. Geiger, J.P. Spatz, A.D. Bershadsky, Environmental sensing through focal adhesions, Nat. Rev. Mol. Cell Biol. 10 (1) (2009) 21–33.
[29] J.T. Parsons, A.R. Horwitz, M.A. Schwartz, Cell adhesion: integrating cytoskeletal dynamics and cellular tension, Nat. Rev. Mol. Cell Biol. 11 (9) (2010) 633–643.
[30] W.T. Chen, Mechanism of retraction of the trailing edge during fibroblast movement, J. Cell Biol. 90 (1) (1981) 187–200.
[31] M. Vicente-Manzanares, X. Ma, R.S. Adelstein, A.R. Horwitz, Non-muscle myosin II takes Centre stage in cell adhesion and migration, Nat. Rev. Mol. Cell Biol. 10 (11) (2009) 778–790.
[32] W. Huang, T.S. Matsui, T. Saito, M. Kuragano, M. Takahashi, T. Kawahara, M. Sato, S. Deguchi, Mechanosensitive myosin II but not cofilin primarily contributes to cyclic cell stretch-induced selective disassembly of actin stress fibers, Am. J. Phys. Cell Phys. 320 (6) (2021) C1153–C1163.
[33] Q.M. Chen, V.C. Tu, J. Catania, M. Burton, O. Toussaint, T. Dilley, Involvement of Rb family proteins, focal adhesion proteins and protein synthesis in senescent morphogenesis induced by hydrogen peroxide, J. Cell Sci. 113 (Pt 22) (2000) 4087–4097.
[34] O. Moujaber, F. Fishbein, N. Omran, Y. Liang, I. Colmegna, J.F. Presley, U. Stochaj, Cellular senescence is associated with reorganization of the microtubule cytoskeleton, Cell. Mol. Life Sci. 76 (6) (2019) 1169–1183.
[35] A.J. Ridley, M.A. Schwartz, K. Burridge, R.A. Firtel, M.H. Ginsberg, G. Borisy, J. T. Parsons, A.R. Horwitz, Cell migration: integrating signals from front to back, Science 302 (5651) (2003) 1704–1709.
[36] S. Tojkander, G. Gateva, P. Lappalainen, Actin stress fibers – assembly, dynamics and biological roles, J. Cell Sci. 125 (8) (2012) 1855–1864.
[37] S. Liu, T.S. Matsui, N. Kang, S. Deguchi, Analysis of senescence-responsive stress fiber proteome reveals reorganization of stress fibers mediated by elongation factor eEF2 in HFF-1 cells, Mol. Biol. Cell 33 (1) (2022) ar10.
[38] S. Di Rubbo, N.G. Irani, S.Y. Kim, Z.Y. Xu, A. Gadeyne, W. Dejonghe, I. Vanhoutte, G. Persiau, D. Eeckhout, S. Simon, K. Song, J. Kleine-Vehn, J. Friml, G. De Jaeger, D. Van Damme, I. Hwang, E. Russinova, The clathrin adaptor complex AP-2 mediates endocytosis of brassinosteroid insensitive1 in Arabidopsis, Plant Cell 25 (8) (2013) 2986–2997.
[39] J. Shin, A. Nile, J.W. Oh, Role of adaptin protein complexes in intracellular trafficking and their impact on diseases, Bioengineered 12 (1) (2021) 8259–8278.

[40] Z. Kadlecova, S.J. Spielman, D. Loerke, A. Mohanakrishnan, D.K. Reed, S. L. Schmid, Regulation of clathrin-mediated endocytosis by hierarchical allosteric activation of AP2, J. Cell Biol. 216 (1) (2017) 167–179.
[41] C. Wang, D. Zhao, S.Z.A. Shah, W. Yang, C. Li, L. Yang, Proteome analysis of potential synaptic vesicle cycle biomarkers in the cerebrospinal fluid of patients with sporadic Creutzfeldt-Jakob disease, Mol. Neurobiol. 54 (7) (2017) 5177–5191.
[42] S. Deguchi, T.S. Matsui, D. Komatsu, M. Sato, Contraction of stress fibers extracted from smooth muscle cells: effects of varying ionic strength, J. Biomech. Sci. Eng. 7 (4) (2012) 388–398.
[43] T. Okamoto, T.S. Matsui, T. Ohishi, S. Deguchi, Helical structure of actin stress fibers and its possible contribution to inducing their direction-selective disassembly upon cell shortening, Biomech. Model. Mechanobiol. 19 (2) (2020) 543–555.
[44] T.S. Matsui, R. Kaunas, M. Kanzaki, M. Sato, S. Deguchi, Non-muscle myosin II induces disassembly of actin stress fibres independently of myosin light chain dephosphorylation, Interface Focus 1 (5) (2011) 754–766.
[45] T. Saito, D. Matsunaga, T.S. Matsui, K. Noi, S. Deguchi, Determining the domain-level reaction-diffusion properties of an actin-binding protein transgelin-2 within cells, Exp. Cell Res. 404 (1) (2021) 112619.
[46] V. Gorgoulis, H. Pratsinis, P. Zacharatos, C. Demoliou, F. Sigala, P. Asimacopoulos, A. Papavassiliou, D., Kletsas, p53-dependent ICAM-1 overexpression in senescent human cells identified in atherosclerotic lesions, Laboratory investigation, J. Techn. Methods Pathol. 85 (2005) 502–511.
[47] C.H. Tsai, C.Y. Chang, B.Z. Lin, Y.L. Wu, M.H. Wu, L.T. Lin, W.C. Huang, J.D. Holz, T.J. Sheu, J.S. Lee, R.N. Kitsis, P.H. Tai, Y.J. Lee, Up-regulation of cofilin-1 in cell senescence associates with morphological change and p27(kip1) -mediated growth delay, Aging Cell 20 (1) (2021) e13288.
[48] A.L. Berrier, K.M. Yamada, Cell–matrix adhesion, J. Cell. Physiol. 213 (3) (2007) 565–573.
[49] W.-T. Chao, J. Kunz, Focal adhesion disassembly requires clathrin-dependent endocytosis of integrins, FEBS Lett. 583 (8) (2009) 1337–1343.
[50] S.M. Schoenwaelder, K. Burridge, Bidirectional signaling between the cytoskeleton and integrins, Curr. Opin. Cell Biol. 11 (2) (1999) 274–286.
[51] M. Chrzanowska-Wodnicka, K. Burridge, Rho-stimulated contractility drives the formation of stress fibers and focal adhesions, J. Cell Biol. 133 (6) (1996) 1403–1415.
[52] S. Sen, S. Kumar, Cell–Matrix De-Adhesion dynamics reflect contractile mechanics, Cell. Mol. Bioeng. 2 (2) (2009) 218–230.
[53] R. Pankov, E. Cukierman, B.-Z. Katz, K. Matsumoto, D.C. Lin, S. Lin, C. Hahn, K. M. Yamada, Integrin dynamics and matrix assembly: tensin-dependent translocation of α5β1 integrins promotes early fibronectin Fibrillogenesis, J. Cell Biol. 148 (5) (2000) 1075–1090.
[54] Z. Gu, E.H. Noss, V.W. Hsu, M.B. Brenner, Integrins traffic rapidly via circular dorsal ruffles and macropinocytosis during stimulated cell migration, J. Cell Biol. 193 (1) (2011) 61–70.
[55] S.J. Lo, L.C. Fan, Y.F. Tsai, K.Y. Lin, H.L. Huang, T.H. Wang, H. Liu, T.C. Chen, S. F. Huang, C.J. Chang, Y.J. Lin, B.Y. Yung, S.Y. Hsieh, A novel interaction of nucleophosmin with BCL2-associated X protein regulating death evasion and drug sensitivity in human hepatoma cells, Hepatology 57 (5) (2013) 1893–1905.
[56] C.M. Kenific, T. Wittmann, J. Debnath, Autophagy in adhesion and migration, J. Cell Sci. 129 (20) (2016) 3685–3693.
[57] J.M. van Deursen, The role of senescent cells in ageing, Nature 509 (7501) (2014) 439–446.
[58] C. López-Otín, M.A. Blasco, L. Partridge, M. Serrano, G. Kroemer, The hallmarks of aging, Cell 153 (6) (2013) 1194–1217.
[59] L. Hayflick, The limited in vitro lifetime of human diploid cell strains, Exp. Cell Res. 37 (1965) 614–636.
[60] J. Tigges, J. Krutmann, E. Fritsche, J. Haendeler, H. Schaal, J.W. Fischer, F. Kalfalah, H. Reinke, G. Reifenberger, K. Stühler, N. Ventura, S. Gundermann, P. Boukamp, F. Boege, The hallmarks of fibroblast ageing, Mech. Ageing Dev. 138 (2014) 26–44.
[61] V.J. Cristofalo, R.J. Pignolo, Molecular markers of senescence in fibroblast-like cultures, Exp. Gerontol. 31 (1–2) (1996) 111–123.
[62] M. Collado, M. Serrano, Senescence in tumours: evidence from mice and humans, Nat. Rev. Cancer 10 (1) (2010) 51–57.
[63] G.P. Dimri, X. Lee, G. Basile, M. Acosta, G. Scott, C. Roskelley, E.E. Medrano, M. Linskens, I. Rubelj, O. Pereira-Smith, A biomarker that identifies senescent human cells in culture and in aging skin in vivo, Proc. Natl. Acad. Sci. 92 (20) (1995) 9363–9367.
[64] J.C. Angello, W.R. Pendergrass, T.H. Norwood, J. Prothero, Proliferative potential of human fibroblasts: an inverse dependence on cell size, J. Cell. Physiol. 132 (1) (1987) 125–130.
[65] Y.M. Kim, H.O. Byun, B.A. Jee, H. Cho, Y.H. Seo, Y.S. Kim, M.H. Park, H.Y. Chung, H.G. Woo, G. Yoon, Implications of time-series gene expression profiles of replicative senescence, Aging Cell 12 (4) (2013) 622–634.
[66] A.C. Lloyd, The regulation of cell size, Cell 154 (6) (2013) 1194–1205.
[67] J.I. Lehtimäki, E.K. Rajakylä, S. Tojkander, P. Lappalainen, Generation of stress fibers through myosin-driven reorganization of the actin cortex, eLife 10 (2021) e60710.
[68] J. Jiao, L. Jiang, Y. Luo, N6-Methyladenosine-related RNA signature predicting the prognosis of ovarian cancer, Recent Pat. Anticancer Drug Discov. 16 (3) (2021) 407–416.
[69] P. Huang, Y.D. Guo, H.W. Zhang, Identification of hub genes in pediatric Medulloblastoma by multiple-microarray analysis, J. Mol. Neurosci. 70 (4) (2020) 522–531.
[70] T. Raj, Y.I. Li, G. Wong, J. Humphrey, M. Wang, S. Ramdhani, Y.C. Wang, B. Ng, I. Gupta, V. Haroutunian, E.E. Schadt, T. Young-Pearse, S. Mostafavi, B. Zhang, P. Sklar, D.A. Bennett, P.L. De Jager, Integrative transcriptome analyses of the aging brain implicate altered splicing in Alzheimer's disease susceptibility, Nat. Genet. 50 (11) (2018) 1584–1592.
[71] Y. Tian, J.C. Chang, E.Y. Fan, M. Flajolet, P. Greengard, Adaptor complex AP2/PICALM, through interaction with LC3, targets Alzheimer's APP-CTF for terminal degradation via autophagy, Proc. Natl. Acad. Sci. USA 110 (42) (2013) 17071–17076.
[72] X. Wang, X. Hu, J. Li, A.C. Russe, N. Kawazoe, Y. Yang, G. Chen, Influence of cell size on cellular uptake of gold nanoparticles, Biomater. Sci. 4 (6) (2016) 970–978.
[73] T.P. Miettinen, M.J. Caldez, P. Kaldis, M. Björklund, Cell size control – a mechanism for maintaining fitness and function, BioEssays 39 (9) (2017) 1700058.
[74] B. Roy, L. Yuan, Y. Lee, A. Bharti, A. Mitra, G.V. Shivashankar, Fibroblast rejuvenation by mechanical reprogramming and redifferentiation, Proc. Natl. Acad. Sci. 117 (19) (2020) 10131–10141.
[75] D. Gill, A. Parry, F. Santos, H. Okkenhaug, C.D. Todd, I. Hernando-Herraez, T. M. Stubbs, I. Milagre, W. Reik, Multi-omic rejuvenation of human cells by maturation phase transient reprogramming, eLife 11 (2022) e71624.
[76] D.H. Kim, D. Wirtz, Focal adhesion size uniquely predicts cell migration, FASEB J. 27 (4) (2013) 1351–1361.
[77] T. Yeung, P.C. Georges, L.A. Flanagan, B. Marg, M. Ortiz, M. Funaki, N. Zahir, W. Ming, V. Weaver, P.A. Janmey, Effects of substrate stiffness on cell morphology, cytoskeletal structure, and adhesion, Cell Motil. Cytoskeleton 60 (1) (2005) 24–34.
[78] K.M. Hakkinen, J.S. Harunaga, A.D. Doyle, K.M. Yamada, Direct comparisons of the morphology, migration, cell adhesions, and actin cytoskeleton of fibroblasts in four different three-dimensional extracellular matrices, Tissue Eng. Part A 17 (5–6) (2011) 713–724.
[79] P. Moreno-Layseca, J. Icha, H. Hamidi, J. Ivaska, Integrin trafficking in cells and tissues, Nat. Cell Biol. 21 (2) (2019) 122–132.
[80] N.R. Paul, G. Jacquemet, P.T. Caswell, Endocytic trafficking of Integrins in cell migration, Curr. Biol. 25 (22) (2015) R1092–R1105.
[81] R.E. Bridgewater, J.C. Norman, P.T. Caswell, Integrin trafficking at a glance, J. Cell Sci. 125 (Pt 16) (2012) 3695–3701.
[82] J.Z. Kechagia, J. Ivaska, P. Roca-Cusachs, Integrins as biomechanical sensors of the microenvironment, Nat. Rev. Mol. Cell Biol. 20 (8) (2019) 457–473.
[83] M. Schuh, An actin-dependent mechanism for long-range vesicle transport, Nat. Cell Biol. 13 (12) (2011) 1431–1436.
[84] K. Kawakami, H. Tatsumi, M. Sokabe, Dynamics of integrin clustering at focal contacts of endothelial cells studied by multimode imaging microscopy, J. Cell Sci. 114 (Pt 17) (2001) 3125–3135.
[85] M.A. Lawson, F.R. Maxfield, Ca2+− and calcineurin-dependent recycling of an integrin to the front of migrating neutrophils, Nature 377 (6544) (1995) 75–79.
[86] A. Arjonen, J. Alanko, S. Veltel, J. Ivaska, Distinct recycling of active and inactive β1 integrins, Traffic 13 (4) (2012) 610–625.
[87] D.A. Calderwood, Y. Fujioka, J.M. de Pereda, B. García-Alvarez, T. Nakamoto, B. Margolis, C.J. McGlade, R.C. Liddington, M.H. Ginsberg, Integrin beta cytoplasmic domain interactions with phosphotyrosine-binding domains: a structural prototype for diversity in integrin signaling, Proc. Natl. Acad. Sci. USA 100 (5) (2003) 2272–2277.
[88] A. Vlahakis, J. Debnath, The interconnections between autophagy and integrin-mediated cell adhesion, J. Mol. Biol. 429 (4) (2017) 515–530.